Leveraging the power of high-parameter cell sorting and single-cell multiomics to profile intratumoral immune cells in a model of B-cell lymphoma

BD FACSymphony™ S6 Cell Sorter and BD Rhapsody™ Single-Cell Analysis System enable a comprehensive analysis of cell composition in the tumor microenvironment

Features

- Simultaneous isolation of 6 immune cell populations from a tumor niche for single-cell profiling
- Integration of single-cell surface protein and gene expression analysis for an in-depth characterization of cell function and phenotype
- Six-way sorting supports a multiomic approach to examine the effects of an inhibitory signaling pathway in B-cell lymphoma

The pathogenesis of B-cell malignancies is a dynamic process involving reciprocal interactions between malignant cells and surrounding components in the tumor microenvironment. In the case of certain B-cell lymphomas, neoplastic B-cells migrate to lymphoid sites and prompt immune cell infiltration. The infiltration of cytotoxic lymphocytes correlates with tumor cell killing and good prognosis. However, most immune cell types in the tumor niche often become unresponsive or even end up promoting tumor growth.

In this study, we examined a murine model of B-cell lymphoma with focus on the function of the B and T lymphocyte attenuator (BTLA) in the progression of the tumor. To investigate cell composition in the

lymphoma microenvironment, we designed a high-throughput sorting strategy to enable concurrent isolation of six cell populations from the tumor niche using the BD FACSymphony S6 Cell Sorter. Then, downstream application of a single-cell multiomic approach was used for a robust characterization of the sorted cell populations.

Figure 1

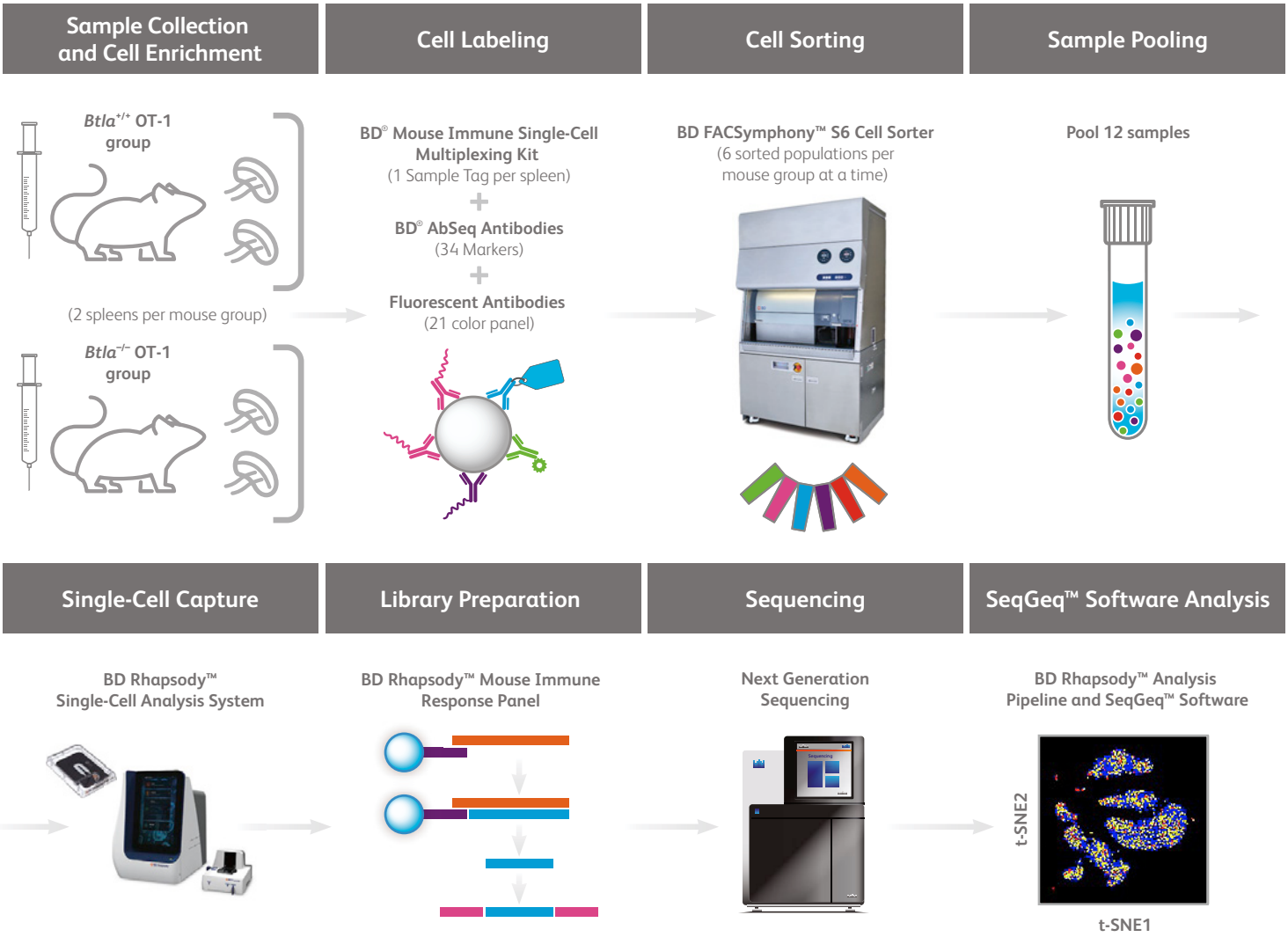

Figure 1. Experimental overview of cell sorting using the BD FACSymphony S6 Cell Sorter and the BD Rhapsody Single-Cell Analysis System workflow.

C57BL/6 mice were inoculated with an ovalbumin-expressing B-cell lymphoma cell line and subsequently with either *Btla*$^{+/+}$ or *Btla*$^{-/-}$ OT-1 T cells. Seven days after the cell transfers, spleens of two mice per group were processed and the cells labeled with BD Pharmingen™ Biotin Rat Anti-Mouse CD19. Then, BD IMag™ Streptavidin Particules Plus-DM were used for magnetic depletion of the CD19^{+} B-cells (not shown). CD19-depleted cells were stained with sample-multiplexing antibodies (1 sample tag per spleen), BD AbSeq Ab-oligos and fluorescent antibodies in the presence of Mouse BD Fc Block™ and BD Horizon™ Brilliant Stain Buffer Plus. The biological replicates from each mouse group were combined in one single tube and six cell populations were sorted from each tube on a BD FACSymphony S6 Cell Sorter. Equivalent numbers of all 12 sorted populations were pooled and loaded (approximately 10,000 cells total) onto the BD Rhapsody Single-Cell Analysis System for single-cell capture. BD AbSeq, mRNA (BD Rhapsody Mouse Immune Response Panel) and sample tag libraries were prepared for sequencing. The sequencing results were analyzed using BD Rhapsody Analysis Pipeline and SeqGeq™ v1.6 Software.

The tissues from B-cell lymphoma–bearing mice were donated by John Sedy and Wai Lin from the Sanford Burnham Prebys Medical Discovery Institute. They induced the tumors by inoculating C57BL/6 mice with an ovalbumin-expressing B-cell lymphoma cell line. Then, in order to investigate tumor-specific immune responses, *Btla*$^{+/+}$ or *Btla*$^{-/-}$ ovalbumin-specific CD8^{+} T cells (OT-1 T cells) were adoptively transferred to the mice seven days later. Single-cell suspensions of splenocytes were stained with the BD Mouse Immune Single-Cell Multiplexing Kit for sample multiplexing, 34 BD AbSeq Ab-oligos and 21 fluorescent antibodies (Tables 1 and 2). The cell subsets were identified in the cell sorter and 6 populations were simultaneously isolated. After sorting of cells from the *Btla*$^{+/+}$ and *Btla*$^{-/-}$ OT-1 groups, the 12 sorted populations were pooled together prior to being loaded onto the BD Rhapsody System.

Table 1. List of BD AbSeq Antibody Oligos

34-plex BD AbSeq Panel	
Marker	Clone
TCR β	H57-597
TCR γδ	GL3
CD8b.2	53-5.8
CD62L	MEL-14
CD197 (CCR7)	4B12
CD103	M290
CD25	PC61
CD69	H1.2F3
CD49a	Hα31/8
CD279 (PD-1)	J43
CD95 (Fas)	JO2
CD162 (PSGL-1)	2PH1
TIGIT	TX99
CD357 (GITR)	DTA-1
CD366 (TIM-3)	5D12/TIM-3
CD223 (LAG-3)	C9B7W
CD49d (VLA-4)	9C10(MFR4.B)
CD54	3E2
H2-kb	AF6-88.5
CD115 (CSF-1R)	T38-320
F4/80	T45-2342
CD274 (B7-H1)	MIH5
Ly-6G and Ly-6C	RB6-8C5
I-A/I-E	M5/114.15.2
CD64 a and b Alloantigens	X54-5/7.1
CD184 (CXCR4)	2B11/CXCR4
CD182 (CXCR2)	V48-2310
CD49b	HMA2
CD1d	1B1
CD335 (NKp46)	29A1.4
KLRG1	2F1
CD137	1AH2
CD90.2	30-H12
CD90.1	HIS51

Table 2. List of fluorochrome-conjugated antibodies used for cell sorting

21 color cell sorting panel		
Fluorochrome	Marker	Clone
BUV805	CD45R/B220	RA3-6B2
BUV737	Ly-6C	AL-21
BUV615	Siglec-F	E50-2440
BUV563	CD272 (BTLA)	HMBT-6B2
BUV496	CD45RB	16A
BUV395	CD8α	53-6.7
BV786	CD90.1	HIS51
BV750	Ly-6G	1A8
BV650	CD23	B3B4
BV570	CD4	GK1.5
BV480	CD90.2	30-H12
BV421	CD44	IM7
BB790	NK1.1	PK136
7-AAD	Live/dead	
BB630	CD11c	HL-3
GFP	Lymphoma Cells	
PE-Cy7	CD11a	2D7
PE	CD5	53-7.3
APC-H7	CD19	1D3
APC-R700	CD11b	M1/70
APC	CD3e	145-2C11

In addition to the transferred OT-1 T cells, we isolated endogenous $CD8^+$ T cells, effector $CD4^+$ T cells, NK cells and two myeloid cell subsets containing Ly-$6G^{high}$ Ly-$6C^{low}$ or Ly-$6G^{low}$Ly-$6C^{high}$ myeloid-derived suppressor cells (MDSCs - Figure 2). We used both BD AbSeq Ab-oligos and fluorescent antibodies anti-CD90.1 and anti-CD90.2 during cell staining. By doing so, we could separate endogenous $CD8^+$ T cells ($CD90.1^-$ $CD90.2^+$) from OT-1 T cells ($CD90.1^+CD90.2^-$, *Btla*$^{+/+}$ group or $CD90.1^+CD90.2^+$, *Btla*$^{-/-}$ group) during cell sorting and downstream analysis (Figures 2B, 3 and 4C).

Figure 2

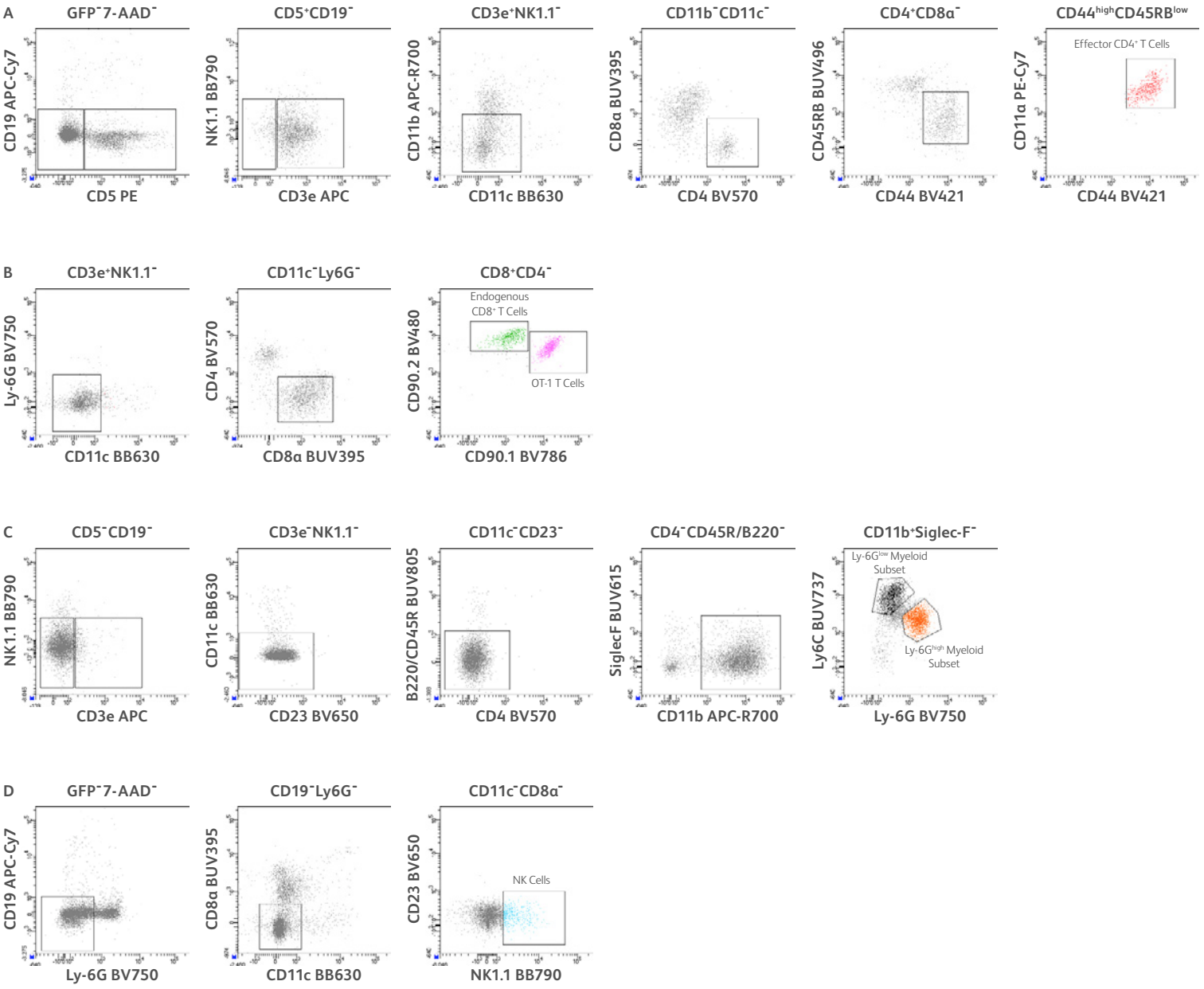

Figure 2. Sorting strategy to enrich 6 different immune cell types using the BD FACSymphony S6 Cell Sorter.

Single-cell suspensions of splenocytes were obtained and stained as described in Figure 1. During acquisition in the sorter, 7-AAD⁺ dead cells, doublets and GFP⁺ lymphoma cells were excluded. Subsequently, six cell populations were identified and selected for sorting. **A)** CD4⁺ effector T cells. **B)** Endogenous CD8⁺ T cells and transferred OT-1 T cells. **C)** Ly-6G^{low}Ly-6C^{high} and Ly-6G^{high}Ly-6C^{low} myeloid subsets. **D)** NK cells. Representative sorting data of cells from the *Btla*$^{-/-}$ group, in which OT-1 T cells are CD90.1⁺CD90.2⁺.

SeqGeq v.1.6 Software was used to perform t-Distributed Stochastic Neighbor Embedding (t-SNE) analysis to visualize the distribution of the 6 sorted cell populations based on expression of conventional mRNA transcripts and proteins (Figure 3). The transferred OT-1 CD8$^+$ T cells could be separated from endogenous CD8$^+$ T cells based on co-expression of *Cd8a* transcript and CD90.1 protein. Effector CD4$^+$ T cells and NK cells were identified based on the expression of *Cd4* and *Klra7*, respectively. Lastly, we used AbSeq Antibodies anti-Ly-6G and Ly-6C (Gr1) and anti-CD115 to distinguish two myeloid subsets of interest.

Figure 3

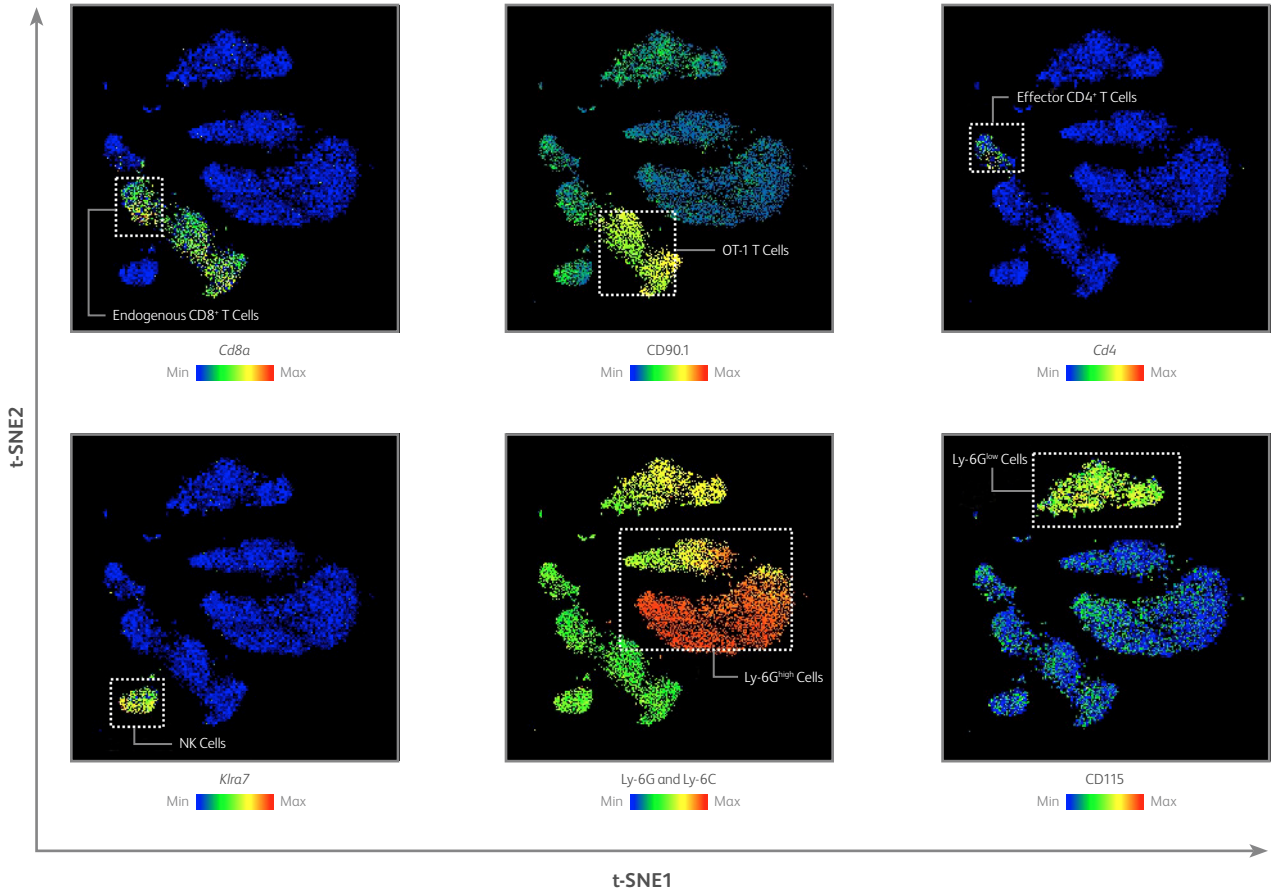

Figure 3. Identification of 6 sorted cell populations using mRNA and protein expression analysis.

The t-SNE plots show the expression of key proteins and mRNA transcripts that were used to depict the 6 sorted populations.

Next, we performed an in-depth characterization of CD8$^+$ T cells to determine changes in protein and mRNA expression upon lymphoma induction. Analysis of the correlated expression of CD90.1 and CD90.2 on gated TCRβ$^+$CD8b$^+$ cells enabled us to distinguish endogenous CD8$^+$ T cells from *Btla*$^{+/+}$ and *Btla*$^{-/-}$ OT-1 T cells (Figure 4). Differential gene and protein expression analysis between transferred OT-1 T cells from the *Btla*$^{+/+}$ (CD90.1$^+$CD90.2$^-$) and *Btla*$^{-/-}$ (CD90.1$^+$CD90.2$^+$) groups revealed a higher expression of CD279 (PD-1) protein in the knockout cells (Figure 4C, heatmap). CD279 signaling controls T-cell mediated immune responses, playing critical roles in tumorigenesis. Thus, this result prompted us to investigate the activation status of endogenous CD8$^+$ T cells as well. To better visualize the data, we applied t-SNE to the TCRβ$^+$CD8b$^+$ cells. The t-SNE plot clearly showed the segregation of endogenous, *Btla*$^{+/+}$ and *Btla*$^{-/-}$ CD8$^+$ T cells (Figure 4D). Next, we separated the two groups of mice for further analysis of protein and mRNA expression. Again, analysis of CD90.1 protein expression could be used to differentiate the transferred from endogenous CD8$^+$ T cells (Figure 4E, top row). Furthermore, the transferred OT-1 T cells , either *Btla* wild type or knockout, could be characterized based on the higher expression of the integrin CD49a (Figure 4E, middle row) as compared to endogenous CD8$^+$ T cells. We also confirmed the upregulation of CD279 on *Btla*$^{-/-}$ OT-1 T cells, as compared to *Btla*$^{+/+}$ OT-1 T cells. Interestingly, CD279 expression was also higher on endogenous CD8$^+$ T cells from the *Btla*$^{-/-}$ group. The t-SNE plot on total

CD8⁺ T cells also revealed distinct clusters on the *Btla*$^{-/-}$group (Figure 4E, bottom). Because these cell clusters belonged to endogenous CD8⁺ T cells (CD90.1⁻CD90.2⁺), we then performed an unbiased clustering analysis using the SeqGeq Software plug-in PhenoGraph for a comprehensive characterization of these cells. Overlay of the PhenoGraph clusters to a t-SNE plot revealed some cell distribution differences between both mice groups (Figure 5A). As an example, while PhenoGraph cluster 4 cells from the *Btla*$^{+/+}$ group were more dispersed on the t-SNE plot, the *Btla*$^{-/-}$ group cells formed a tighter cluster. Differential protein and mRNA analysis showed that a majority of the cluster 4 cells from the *Btla*$^{-/-}$ group had a distinct signature, with cells co-expressing CD279 and CD137 (Figure 5B). Furthermore, differential expression analysis between the individual clusters in the *Btla*$^{-/-}$ group revealed the heterogeneity of endogenous CD8⁺ T cells based on unique patterns of protein and mRNA expression, shown in the representative heatmap in Figure 5C.

Figure 4

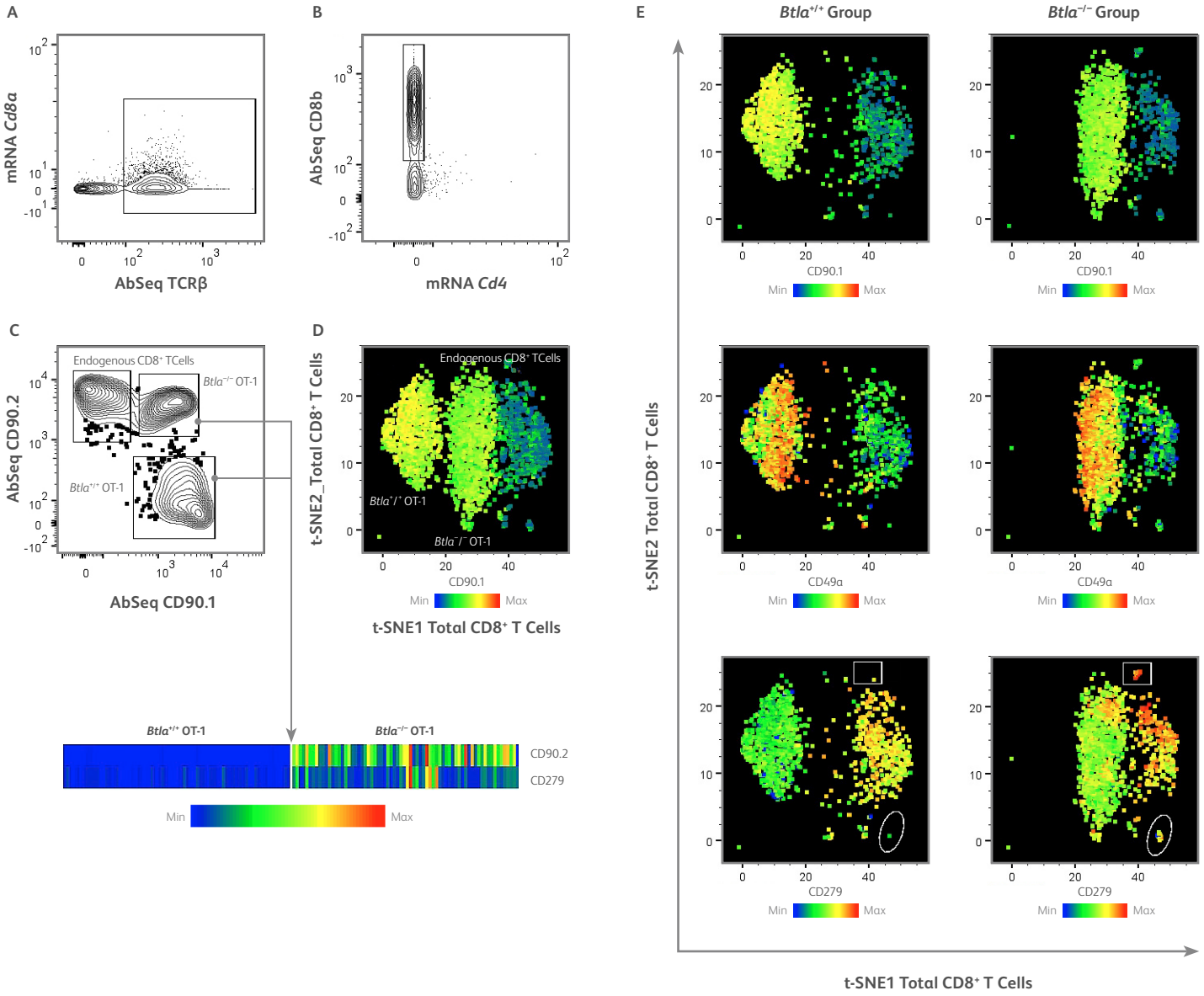

Figure 4. Clustering analysis showing the differences between the transferred OT-1 T cells and endogenous CD8⁺ T cells from lymphoma-bearing mice.

A and B) Identification of total CD8⁺ T cells by manual gating on TCRβ⁺*Cd8a*⁺CD8b⁺ cells. **C)** Contour plots of CD90.1 and CD90.2 surface protein expression and heatmap showing differential protein expression between *Btla*$^{+/+}$ (CD90.1⁺CD90.2⁻) and *Btla*$^{-/-}$ (CD90.1⁺CD90.2⁺) OT-1 T cells. **D)** t-SNE coordinates of total CD8⁺ T cells showing expression of CD90.1. Analysis of CD90.2 expression in the t-SNE plot (not shown) was also used to facilitate the identification of the clusters. **E**) Comparison between the two groups of mice based on the analysis of key markers on the total CD8⁺ T cells. The circle and square gates identify clusters that were observed only in the *Btla*$^{-/-}$ group.

Figure 5

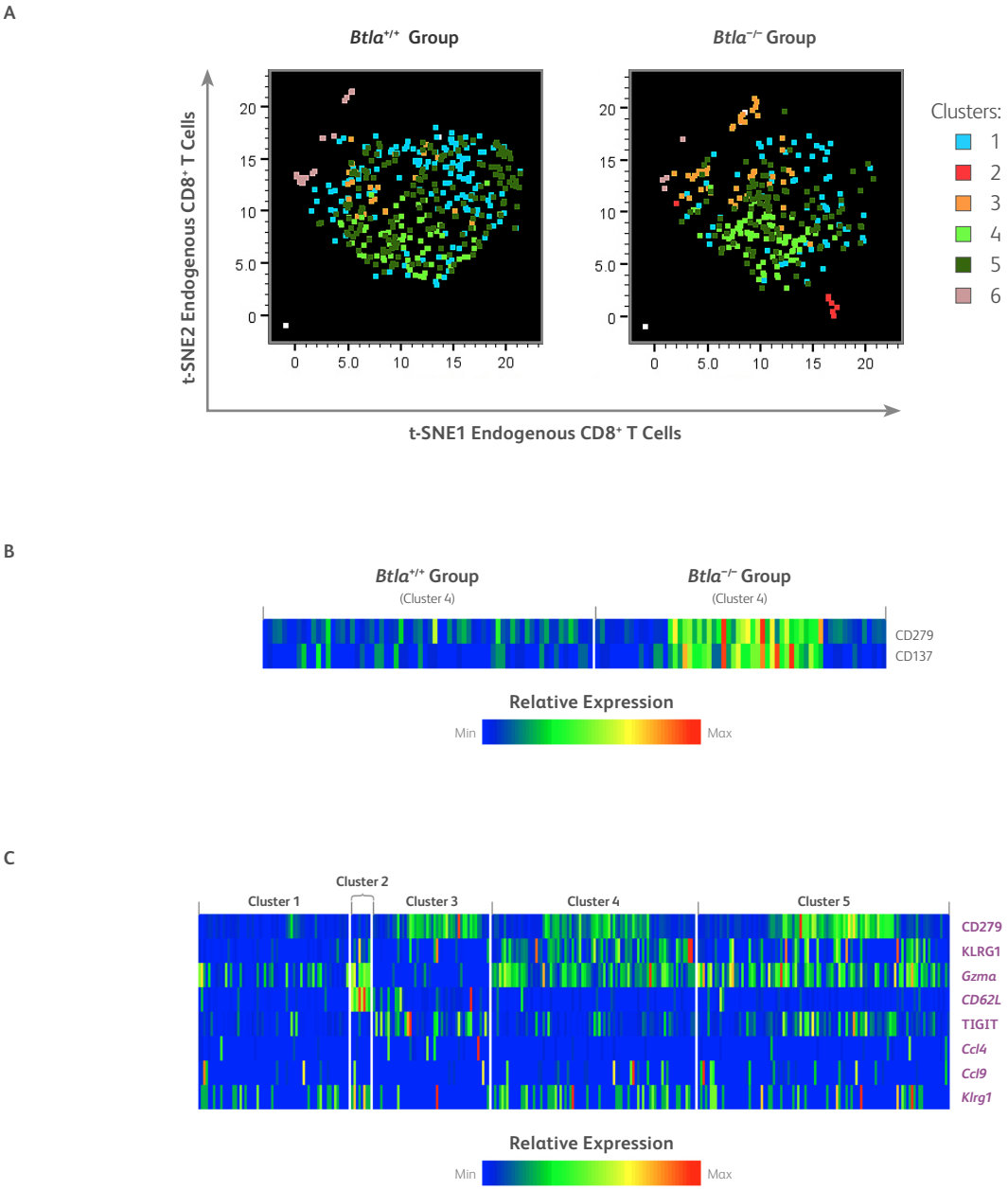

Figure 5. Clustering analysis showing depth characterization of endogenous CD8⁺ T cells in B-cell lymphoma-bearing mice.

A) Unsupervised clustering of endogenous CD8⁺ T cells using PhenoGraph identified six cell clusters projected on the t-SNE map. **B)** Heatmap of PhenoGraph cluster 4 showing upregulation of CD279 and CD137 in the *Btla*$^{-/-}$ group compared to the *Btla*$^{+/+}$ group. **C)** Heatmap showing a set of proteins and mRNA transcripts that were detected in the PhenoGraph clusters of endogenous CD8⁺ T cells from the *Btla*$^{-/-}$ group.

In summary, we demonstrated an approach that enabled a thorough characterization of critical cell populations in tumor responses. Our analyses revealed that the loss of BTLA function may increase the proportions of CD8⁺ T cells that express CD279 as a response to the onset of B-cell lymphoma in a mouse model. This was observed in lymphoma-specific CD8⁺ T cells that were transferred to mice with tumors as well as in endogenous CD8⁺ T cells. Furthermore, the endogenous cells expressed a series of proteins and mRNA transcripts, including CD137 and *Gzma* that suggested they had undergone activation and may contribute to eliminating the tumor cells. Further analyses of the remaining sorted populations may shed light on the interplay of different immune cell types in B-cell lymphoma. Because these cell populations constitute potential targets for the treatment of the disease, the described workflow combining high-parameter cell sorting with single-cell multiomics may offer an opportunity for identification of new therapeutic targets.

BD Life Sciences – Biosciences Regional Offices

bdbiosciences.com/contact

Australia
Toll free 1.800.656.100
Tel 61.2.8875.7000
Fax 61.2.8875.7200

Canada
Tel 866.979.9408
Fax 888.229.9918

China
Tel 86.21.3210.4610
Fax 86.21.5292.5191

Europe
Tel 32.2.400.98.95
Fax 32.2.401.70.94

India
Tel 91.124.2383566
Fax 91.124.2383224/25/26

Japan
Nippon Becton Dickinson
Toll free 0120.8555.90
Fax 81.24.593.3281

Latin America / Caribbean
Toll free 0800.771.71.57
Tel 55.11.5185.9688

New Zealand
Toll free 0800.572.468
Tel 64.9.574.2468
Fax 64.9.574.246

Singapore
Tel 65.6690.8691
Fax 65.6860.1593

United States
U.S. orders 855.236.2772
Technical Service 877.232.8995
Fax 800.325.9637

Office locations are available on our website.

Class 1 Laser Product.
For Research Use Only. Not for use in diagnostic or therapeutic procedures.
23-22482-00

BD Life Sciences, San Jose, CA, 95131, USA

bdbiosciences.com